Environmental Science and Pollution Research (2024) 31:3598–3613
https://doi.org/10.1007/s11356-023-31345-3

RESEARCH ARTICLE

Monitoring agricultural drought in Peshawar Valley, Pakistan using long -term satellite and meteorological data

Tehseen Javed[1,2,3] · Nishan Bhattarai[4] · Bharat Sharma Acharya[5] · Jiahua Zhang[1,6]

Received: 18 July 2023 / Accepted: 30 November 2023 / Published online: 12 December 2023
© The Author(s), under exclusive licence to Springer-Verlag GmbH Germany, part of Springer Nature 2023

Abstract

Monitoring agricultural drought across a large area is challenging, especially in regions with limited data availability, like the Peshawar Valley, which holds great agricultural significance in Pakistan. Although remote sensing provides biophysical variables such as precipitation (P), land surface temperature (LST), normalized difference vegetation index (NDVI), and relative soil moisture (RSM) to assess drought conditions at various spatiotemporal scales, these variables have limited capacity to capture the complex nature of agricultural drought and associated crop responses. Here, we developed a composite drought index named "Temperature Vegetation ET Dryness Index" (TVEDI) by modifying the Temperature Vegetation Precipitation Dryness Index (TVPDI) and integrating NDVI, LST, and remotely sensed evapotranspiration (ET) using 3D space and Euclidean distance. Several statistical techniques were employed to examine TVPDI and TVEDI trends and relationships with other commonly used drought indices such as the standardized precipitation index (SPI), standardized precipitation evapotranspiration index (SPEI), and standardized soil moisture index (SSI), as well as crop yield, to better understand how these indices captured the spatial and temporal distribution of agricultural drought in the Peshawar valley between 1986 and 2018. Results indicated that while the temporal patterns of the 3-month SPI, SPEI, and SSI generally align with those of TVEDI and TVPDI, TVEDI was more strongly correlated with these indices (e.g., correlation coefficient, $r = 0.78–0.84$ from TVEDI and $r = 0.73–0.79$ from TVPDI). Moreover, the crop yield, a measure of crop response to agricultural drought, demonstrated a significant positive correlation with TVEDI ($r = 0.60–0.80$), much higher than its correlation with TVPDI ($r = 0.30–0.48$). These outcomes indicate that the inclusion of ET in TVEDI effectively captured changes in soil moisture, crop water status, and their impact on crop yield. Overall, TVEDI exhibited enhanced capability to identify drought impacts compared to TVPDI, showing its potential for characterizing agricultural drought in regions with limited data availability.

Keywords Agricultural Drought · Auto-correlation · Evapotranspiration · TVEDI · And TVPDI

Introduction

Studying drought is essential for comprehending, understanding, and addressing the profound consequences of water scarcity on agriculture, ecosystems, and human societies to ensure the stability of food supplies and ecological

Responsible Editor: Rongrong Wan

✉ Jiahua Zhang
jhzhang@ceode.ac.cn

Tehseen Javed
tehseenjaved@nwafu.edu.cn

[1] Remote Sensing Information and Digital Earth Center, School of Computer Science and Technology, Qingdao University, Qingdao 266071, China

[2] School of Business, Qingdao University, Qingdao 266071, China

[3] Department of Environmental Sciences, Kohat University of Science & Technology, Kohat 26000, KPK, Pakistan

[4] Department of Geography and Environmental Sustainability, the University of Oklahoma, Norman 73019, USA

[5] Rodale Institute Southeast Organic Center, Chattahoochee Hills, GA 30268, USA

[6] Key Laboratory of Digital Earth Science, Aerospace Information Research Institute, Chinese Academy of Sciences, Beijing 100094, China

equilibrium under climate change (Chen et al. 2020; Edwards et al. 1997; Fatemi and Narangifard 2019; Henchiri et al. 2020). The Sixth Assessment Report (AR6) of the Intergovernmental Panel on Climate Change (IPCC) suggests that drought frequency and intensity will continually increase in the future (IPCC 2021; Pachauri et al. 2014). Drought monitoring and its impact assessments are crucial for developing inclusive drought adaptation and mitigation strategies to support global food security and sustainable development goals (Hao and AghaKouchak 2013; Javed et al. 2021a). Drought monitoring is critical for many regions, including Pakistan, one of the most climate-vulnerable and agriculture-dependent countries in the world, where drought is a common phenomenon. Droughts and extreme events have adversely affected Pakistan's agricultural production, livelihood, and economy in the past (Hussain et al. 2021; Khan et al. 2020). The Climate Risk Index 2021 reported that Pakistan ranked eighth among the most vulnerable and affected countries by extreme climate events between 2000 and 2019, making it a global hotspot for drought research (Jaafar and Ahmad 2020; Khan et al. 2019b).

Drought can be categorized into various types (e.g., meteorological, hydrological, ecological, etc.) based on their specific characteristics and impacts (i.e., reductions in water supply and hydropower generation, disturbance in ecological balance (Mishra and Singh 2010). Agricultural drought is specifically related to the impacts of water scarcity on agricultural production. It is often associated with reduced precipitation, warmer temperatures, increased potential evapotranspiration (PET), and decreased soil moisture (SM), leading to reduced yields (Kwon et al. 2019; Sims et al. 2002). While meteorological and hydrological conditions triggering agricultural and general types of drought, such as meteorological, hydrological, and ecological droughts are similar, agricultural drought tends to be more localized and short-term, often limited to specific regions or cropping seasons (Khan et al. 2019a; Madugundu et al. 2017). In contrast, general drought can persist for longer durations and have more extensive societal and economic consequences, with widespread job losses, reduced GDP, and increased government expenditures on relief efforts (Soľáková et al. 2014; Tasumi 2019). Agricultural drought also affects rural communities due to reduced agricultural income, food scarcity, and migration, linking it directly with another type of drought named socioeconomic drought where the livelihood of rural communities is negatively affected (Khan et al. 2019a; Madugundu et al. 2017). Hence, agricultural drought is a key threat to not only crop production but also the livelihood of people dependent on agriculture (Hussain et al. 2021). A prime example is the recent drought events during 2017- 2018 in Pakistan that affected five million people threatening the country's food security (Khan et al. 2020). Mitigation strategies for agricultural drought often involve crop diversification, irrigation, and drought-resistant crop varieties to safeguard food production (dos Santos et al. 2022; Fadholi and Adzani 2018). Implementing agricultural drought mitigation strategies requires proper characterization of drought conditions and monitoring tools to identify regions under drought that require potential interventions. However, in data-scare regions like Pakistan, developing a drought monitoring tool is a challenge, given that observed weather data are not readily available or nonexistent. Hence, freely available remotely sensed data appears to be the only viable option for monitoring agricultural drought and its impacts in Pakistan (Abramowitz and Stegun 1965; Chen et al. 2013).

To monitor agricultural drought, various remote sensing-based indices or indicators have been proposed. A non-exhaustive list of examples includes the Normalized Difference Vegetation Index (NDVI), Temperature Condition Index (TCI), Soil Moisture Condition Index (SMCI), Vegetation Condition Index (VCI), Precipitation Condition Index (PCI), and Vegetation Health Index (VHI) (Govil et al. 2020; Guha et al. 2018; Musie et al. 2019). Additionally, meteorological drought indicators combining indices from readily available remote sensing or reanalysis-based climate data have also been found to be effective in monitoring agricultural drought across different scales (Javed et al. 2021b; Liu et al. 2020; Henchiri et al. 2020). Among these, Wei et al. (2020), a recently developed Temperature Vegetation Precipitation Dryness Index (TVPDI) that incorporates precipitation, NDVI, and LST demonstrated its potential utility to derive the spatiotemporal pattern of the dryness-wetness status over China at both monthly and annual scales. Though ET is a significant component of the hydrologic budget and a good measure of the water requirement of actively growing vegetation (Liu et al. 2021), it is not widely incorporated in drought indices because of the uncertainty in deriving ET products (Bhattarai et al. 2017). Remote sensing offers a unique opportunity for mapping ET from field to regional scales (Henchiri et al. 2020; Liu et al. 2020; Anderson et al. 2012; Bhattarai et al. 2018). Several remote sensing-based methods exist to map ET across agricultural landscapes, but no model has been found to work best under all conditions (Bhattarai et al. 2016; Bhattarai et al. 2019). Nonetheless, ET-based drought indices are found to characterize vegetation water status efficiently, as ET is a direct vegetation response to water stress (Bhattarai et al. 2017; Bhattarai et al. 2019). Hence, ET is considered a key indicator in creating an integrated drought index to accurately characterize agricultural drought (Anderson et al. 2016; Yang et al. 2018).

In this study, we integrated remotely sensed ET with NDVI and LST to modify TVPDI (Wei et al. 2020) into a new dryness index named Temperature Vegetation Evapotranspiration Dryness Index (TVEDI) and evaluated it against the other common drought indices and yield

anomalies in Peshawar Valley, Pakistan. Through this comparison, we evaluated TVEDI's potential to monitor agricultural drought and its severity in our study region. The primary objective of the study is to assess the performance of TVEDI and TVPDI in characterizing the spatiotemporal variation of dryness and wet conditions and predicting agricultural drought across the study area. Developing a remotely sensed ET-based drought index is important for this region, as current drought mitigation plans in Pakistan mainly focus on using common meteorological and hydrological drought indices (e.g., Standard Precipitation Index (SPI), Standardized Precipitation Evapotranspiration Index (SPEI)) that have limited capability to assess agricultural drought and their negative impacts on crop yield (Ying et al. 2023a; Henchiri et al. 2020; Liu et al. 2020). Through this new tool, this study is expected to provide valuable information to stakeholders and policymakers for mitigating agricultural drought and managing water resources, especially in the irrigated areas of Pakistan.

Materials and methods

Description of the study area

Our study region is the Peshawar Valley, a key wheat and maize-producing region of Pakistan. The valley is situated in the central part of the Khyber Pakhtunkhwa province, expanding over 1,176 km^2, covering a section of River Kabul (Fig. 1). The geographical location is between 33° 50'-34° 01' N and 71° 20'-71° 60' E and has an elevation of 345 m (1,132 ft.). The climate is hot and semi-arid, with scorching summers and mild and cool winters. The mean minimum and maximum temperatures range from 25 °C-40°C in summer and 4 °C to 18.3 °C in winter, respectively. The average annual precipitation is about 530 mm, most of which occurs during summer, and the variation in the precipitation between the driest and wettest months (November/December and, July/August, respectively) is about 141 mm.

Datasets

A total of 632 near cloud-free Landsat satellite images (Landsat 4, 5 TM, Landsat 7ETM$^+$, and Landsat 8 OLI/TIRS) (Fig. 2) covering the study region were obtained from the USGS Earth Explorer website (https://earthexplorer.usgs.gov). The cloud masking and gap-filling procedures Jaafar and Ahmad (2020) suggested were used to process these images. The Landsat images were used to calculate NDVI, LAI, LST, and ET. The Climate Hazards Group Infra-Red Precipitation and Station (CHIRPS-2.0) from 1982–2018 daily precipitation data (0.05° × 0.05°; (https://data.chc.ucsb.edu/products/CHIRPS-2.0/) were used to calculate the SPI (Javed et al. 2021a). Scanning Multichannel Microwave Radiometer (SMMR) and Special Sensor Microwave Imager (SSM/I) datasets (2.5° × 2.5°) were used to obtain soil moisture, and these datasets were obtained from https://climatedataguide.ucar.edu/climate-data. The standardized soil moisture index (SSI) was calculated using the soil moisture datasets (Baig et al. 2020; Hao and Aghakouchak 2013). Regional metrological center Peshawar, climate datasets were used to calculate the SPEI https://

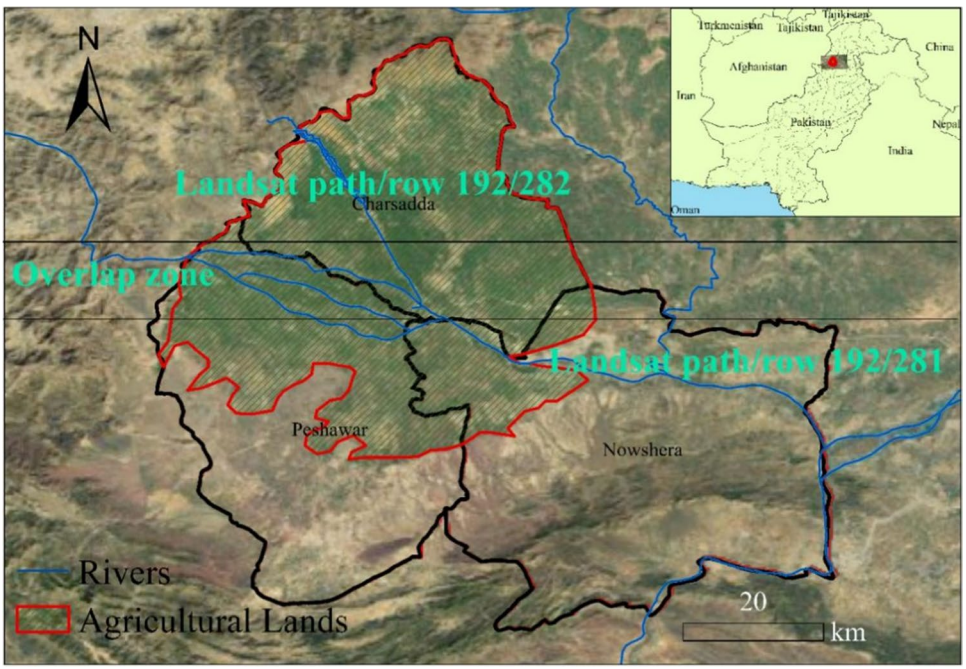

Fig. 1 The study area and the agricultural regions in the Peshawar Valley shown over two Landsat scenes (Path/row 192/282 and 192/281)

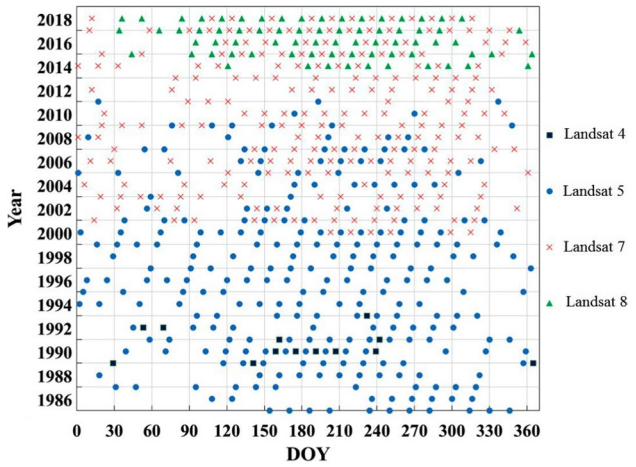

Fig. 2 Cloud-free Landsat (Landsat 4, L4 to Landsat 8, L8) scenes (from path/row 192/281- 192/281) used in this study

rmckpk.pmd.gov.pk/. The datasets were resampled using the bilinear method to bring all datasets into a common spatial resolution of 30 m (Javed et al. 2021). The Tehsil level yield of wheat and maize crops was obtained from the Bureau of Statistics Khyber Pakhtunkhwa Pakistan (https://kpbos.gov.pk).

Methods

Evapotranspiration (ET) Estimation

To estimate the ET for agricultural land, we used the Mapping ET at high Resolution with Internalized Calibration (METRIC) model (Allen et al. 2007), a widely used ET model designed for mapping ET across agricultural lands (Tasumi 2019; Bhattarai et al. 2016 and 2019). The key remote sensing inputs in the model include thermal, visible, and near-infrared bands obtained from Landsat images (Numata et al. 2017). The level 2 Landsat surface reflectance products and pixel quality assurance band (BQA) were obtained from USGS (Liu et al. 2021). The Shuttle Radar Topography Mission (SRTM) digital elevation model (DEM) was used to generate slope and aspect to correct LST or surface temperature (T_s). Meteorological data were obtained from 1986–2018 from the Pakistan Meteorological Department (https://www.pmd.gov.pk/en/). The METRIC model was applied on all near cloud-free Landsat images from January 1986 to December 2018. While the readers are referred to Allen et al. (2007) for model details of the METRIC model, a summary of the model is provided below:

In METRIC and other surface energy balance models, ET or latent heat flux (λE), is derived as the residual of the surface energy balance equation:

$$\lambda E = R_n - G - H \tag{1}$$

where Rn is the net radiation, G is the soil heat flux, H is the sensible heat flux, and λE is the latent heat flux (all units in W m^{-2}). Rn was calculated using the radiation balance equation (Allen et al. 2007). G was calculated using He et al. (2017) as:

$$G = \left\{ \begin{array}{c} \left(0.05 + 0.1 \times e^{-0.52 \times LAI}\right) R_n | LAI \geq 0.5) \\ \left[\left(1.8\left(T_{s_{datum}} - 273.15\right) R_n + 0.084\right)\right] R_n | LAI < 0.5) \end{array} \right\} \tag{2}$$

The Leaf Area Index (LAI) was derived using Zheng and Monika Moskal (2009). In METRIC, sensible heat flux (*H*) is estimated using an iterative process by simultaneously solving equations for *H*, aerodynamic resistance (r_{ah}) from a roughness length for heat transfer plus displacement height ($z_{0h} + d_0$) to the reference height (z), and frictional velocity (u_*) (Eqs. 4–6) and stability functions (Allen et al. 2007) using Monin–Obukhov similarity theory (Businger et al. 1971, Brutsaert 1999) from hot and cold pixels:

$$r_{ah} = \frac{1}{Ku_*}\left[\ln\left(\frac{z - d_0}{z_{0h}}\right) - \psi_{h(z\text{-}d_0)} + \psi_{h(z_{0h})}\right], \tag{4}$$

$$u_* = \frac{Ku_b}{\ln\left(\frac{z - d_0}{z_{0m}}\right) - \psi_m} \tag{5}$$

$$H = \left(\rho_a c_p dt\right) / r_{ah} \tag{6}$$

where ρ_a is the air density (1.15 kg/m^3), c_p is the air-specific heat (1004 J/kg/K), *dT* (K) is the near-surface temperature difference, and $\psi_{h(z_{0h})}$ and $\psi_{h(z\text{-}d_0)}$ are stability functions (Allen et al 2007). *dT* was estimated using a linear relationship between *dT* and LST (T_s) at hot and cold pixels as:

$$dT = a + bT_{s_{datum}} \tag{6}$$

The *a* and *b* are coefficients for each image and were estimated as:

$$a = \frac{dT_{hot} - dT_{cold}}{T_{s\ \text{datum hot}} - T_{s\ \text{datum cold}}} and, b = \frac{(dT_{hot} - a)}{T_{s\ \text{datum hot}}} \tag{7}$$

A hot pixel (H_{hot} = Rn-G) was selected from a dry, bare agricultural field, while a cold pixel ($H_{cold} = R_n$-*G*-1.05λET_r, where ETr is the reference ET during image time) was selected from a well-irrigated crop pixel (Senay et al. 2016). The initial value of *H* from hot and cold pixels is used to calculate dT and was updated using Eq. 4–7 until the difference in *dT* from the hot pixel in the successive iteration is less than 5%. Daily ET (ET_{24}; mm/hr) is estimated using Eq. 7 assuming that the ET fraction (f_{RET}), the ratio of instantaneous ET to reference ET, is constant throughout the day.

$$ET_{24} = C_{rad} \times f_{RET} \times ET_{o24} \quad (8)$$

C_{rad} is the correction coefficient that minimizes the latitude (mountainous terrain) error. The correction coefficient is calculated using the following equation.

$$C_{rad} = \frac{R_{so(inst)Horizontal}}{R_{so(inst)pixel}} \times \frac{R_{so(24)pixel}}{R_{so(24)Horizontal}} \quad (9)$$

where R_{So} represents the clear-sky solar radiation (WM^{-2}), $R_{so\ (inst)}$ is for the horizontal surface, and R_{so} ("inst") pixel is the pixel slope at viaduct (subscript "inst") for the daily time step (subscript "24"). For the correction of 24-h ET terrain, the slope and aspect were calculated using the DEM. Further, the solar angle (latitude, declination, solar zenith angle, and solar angle) was calculated to adjust z_{om} and T_s.

Because observation flux tower or lysimeter ET data was not available, we compared METRIC using monthly ET data available from the Regional Meteorological Center (RMC) in Peshawar. For this comparison, daily ET from the METRIC model was summed to derive monthly ET. RMC uses the FAO CROPWAT model (FAO 2009), which utilizes the Penman–Monteith equation, integrating various parameters like geographic coordinates, surface temperature, relative humidity, wind speed, and solar radiation to determine reference and crop evapotranspiration across different environmental conditions, crops, and soil types. The model has been validated across the globe; however, it is not feasible to implement on Landsat like METRIC. Hence, we aggregated METRIC ET spatially (state-level) and temporally (monthly) and compared it with reported CROPWAT ET from the RMC.

Drought indices calculation

Soil moisture (SM) has a direct influence on vegetation dryness. Precipitation directly affects SM while ET, vegetation health, and LST reflect SM. These four factors combinedly represent dryness or wetness. Hence these four variables were combined to build two 3D spaces (i.e., precipitation, or ET, NDVI, and LST) and monitor the dryness, as depicted in Fig. 3.

To predict the Temperature Vegetation Precipitation Dryness Index (TVPDI) and Temperature Vegetation Evapotranspiration Dryness Index (TVEDI), the Euclidean distance and dryness principal method was utilized. Euclidean distance methods are commonly used to calculate the multidimensional absolute distance between two points (Danielsson 1980; Wang et al. 2005). The Euclidean distance method is widely used in drought monitoring (Javed et al. 2020) and

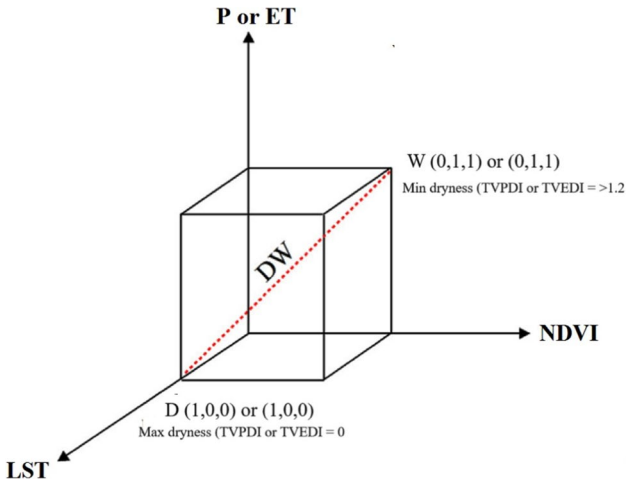

Fig. 3 The development of the TVEDI or TVPDI in a 3D space. W denotes the wettest point, which has the minimum temperature (minimum LST), maximum vegetation cover (maximum NDVI), and maximum P, or ET. In contrast, minimum NDVI, maximum LST, and minimum ET, point D represent the driest point

ecological studies (Vicente-Serrano et al. 2012), and remote sensing imagery processing (Wang et al. 2005). The following expression was used to predict the Euclidean distance:

$$D(X,Y) = \sqrt{\sum_{i=1}^{n} (x_i - y_i)^2} \quad (10)$$

where D (X, Y) is the distance between points X and Y.

To calculate the TVPDI and TVEDI, first, a reference point was set within the multifaceted space, each variable was normalized, and an Euclidean distance method was used to calculate the composite drought index (Wei et al. 2020). Before normalization, the cumulative probability of the dichotomy method was used to minimize outliers' errors:

$$NormalizedX = \frac{X - X_{\min}}{X_{\max} - X_{\min}} \quad (11)$$

where X is either LST, NDVI, P, or ET, and subscripts "min" and "max denote the minimum and maximum values of X for a particular pixel, respectively.

Consequently, based on Euclidean distance, normalized precipitation (NP) or normalized evapotranspiration (NET), normalized NDVI (NNDVI), and normalized LST (NLST) were aggregated to calculate the TVPDI (using NP) and TVEDI (using NET instead of NP). Figure 4 shows the 3D space, where point D is the driest, and point W is the wettest pixel. The points (1, 0, 0, and 1, 0, 0) are the driest reference points, showing the highest LST, lowest NDVI, lowest precipitation, or highest ET. The dryness and wetness range from 0 to 1.5, where 0 suggests maximum dryness and 1.5

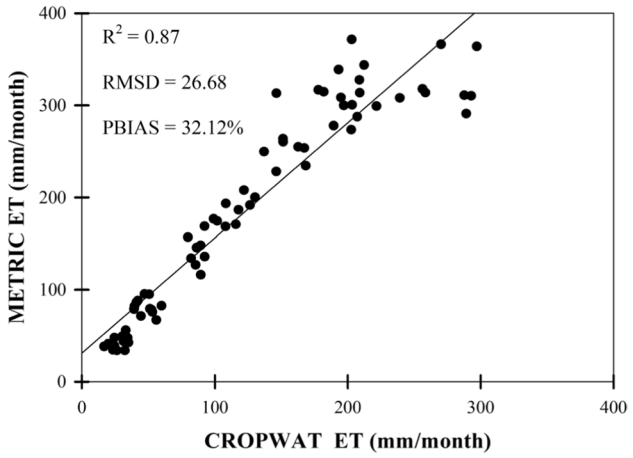

Fig. 4 Scatterplot of monthly ET between FAO CROWAT and METRIC ET models. Each point shows the monthly ET for the state

suggests minimum dryness. The TVPDI and TVEDI were calculated using the following equations.

$$TVPDI = \sqrt{(NLST_{\max} - NLST)^2 + (NNDVI - NNDVI_{\min})^2 + (NP - NP_{\min})^2} \quad (12)$$

$$TVEDI = \sqrt{(NLST_{\max} - NLST)^2 + (NNDVI - NNDVI_{\min})^2 + (NET - NET_{\min})^2} \quad (13)$$

where subscripts "min" and "max denote the minimum and maximum values of a variable for a particular pixel, respectively.

Calculation of SPI, SPEI, and SSI

The precipitation, potential evapotranspiration (PET), and soil moisture data were transformed into a normal distribution to calculate SPI, SPEI, and SSI. The widely used gamma distribution approach was used to derive the probability density function of SPI or SSI.

$$g(x) = \frac{1}{\beta^{\alpha}\Gamma(\alpha)} x^{\alpha-1} e^{-x/\beta} \quad (14)$$

In Eq. 14, α is a shape parameter (α > 0), and β is a scale parameter (β > 0) (Thom 1958). The Γ (α) is the gamma function, denoted as $\int_0^{\infty} y^{\alpha-1} e^{-y} dy$, and x is the precipitation and soil moisture. The SPEI was calculated using the Vicente-Serrano et al. (2010) method. The threshold values for characterizing different categories of drought using SPI, SPEI, and SSI are shown in Table 1.

Table 1 Drought classification by SPI, SPEI, and SSI values

SPI or SPEI or SSI	Category
≥ 2.00	Extremely wet
1.50 to 1.99	Severely wet
1.00 to 1.49	Moderately wet
0.00 to 0.99	Mild wet
-0.99–0.00	Mild drought
-1.49 to -1.00	Moderate drought
-1.99 to -1.50	Severe drought
≤ -2.00	Extreme drought

Statistical analysis

The modified Mann–Kendall test, person correlation, percentage change, and coefficient of variation were used to calculate the significance, linear correlation, linear trend, and stability of the proposed drought index and compare it with other indices. The modified Mann–Kendall test was calculated using (Kendall 1976; Mann 1945; Yue and Wang 2002), and Javed et al. (2020) procedure. The modified Mann–Kendall can be expressed as follows.

$$Z^* = Z/\sqrt{n_1^s}, where n_1^s = \begin{cases} 1 + \frac{1}{n_1}\sum_{jj=1}^{n_1-1}(n_1-1)r_{jj} & for\ jj > 1 \\ 1 + 2\frac{r_1^{n_1+1} - n_1 r_1^2 + (n_1-1)r_1}{n_1(r_1-1)^2} & for\ jj = 1 \end{cases} \quad (15)$$

where Z is considered significant positive or negative when |Z| or |Z* | ≥ ± 1.96 at a confidence level of 0.05 (Javed et al. 2020).

The TVEDI and TVPDI represent surface dryness and wetness, while SPI, SPEI, and SSI are direct metrological and agricultural dryness or wetness indicators that trigger surface dryness or wetness. Therefore, the correlation between SPI, SPEI, and SSI with TVEDI and TVPDI can specify the ability of the TVEDI or TVPDI to monitor surface dryness and wetness (Wei et al. 2020). For the correlation analysis, Pearson correlation coefficient (r) was used between TVEDI and TVPDI other drought indices and crop yield.

Results

Validation of ET from the METRIC model

METRIC monthly ET was able to capture CROPWAT ET during both dry and wet periods, as it was able to explain an 87% variation in CROPWAT monthly ET (Fig. 4). The root mean squared difference (RMSD) between monthly ET from the two models was about 27 mm/month and within 32.12%. This result indicates that remotely sensed ET from the METRIC model was able to represent actual ET on the ground.

Spatiotemporal variation of remotely sensed variables from 1986 to 2018

Monthly NDVI, LST, and ET in the study area showed a similar temporal pattern from 1986 to 2018 depicting clear evidence of their seasonality (Fig. 5). For example, the lowest NDVI, LST, and ET values (0.03, 2˚C, and 1 mm/month) were observed during the winter season, while the highest values (0.78, 32°C, and 283.9 mm/month) were observed in the summer. Though precipitation is a key factor contributing to soil moisture, there was no clear evidence showing the influence of precipitation on soil moisture, suggesting the potential influence of irrigation on soil moisture. The year 2000 was a dry year with 213 mm of precipitation, while the year 2015 was relatively wet with an annual precipitation of 560 mm. This corresponds well with the lowest RSM (40%) in 2000 and the highest RSM (78%) in 2015.

The long-term (1986–2018) average precipitation, NDVI, LST, ET, and RSM across the Peshawar valley are shown in Fig. 6. Generally, the highest precipitation (> 140 mm) occurred in the early spring and monsoon seasons during March, July, and August, particularly in the Northern and Eastern parts of the Peshawar Valley. The lowest precipitation (< 20 mm) occurred in the late autumn and winter, particularly across the Eastern and Southern regions. The lowest NDVI values (0.20–0.40) were observed during the early Rabi season (November to December), and the highest values (0.60- > 0.80) were observed during the mid-Kharif season (August and September) across most of the study area. The highest LST > 40°C was observed during summer across the Northwest and South, and the lowest LST (< 10°C) was observed during winter across the East of the study area. ET values in the Rabi growing season range from 50 to 150 mm/month, while ET values in the Kharif season range from 150 to > 250 mm/month. The RSM lowest value of < 20% was observed in August across the South and Northeast regions, and the highest values (> 80%) were observed mainly in the Northeast and Southeast of the study area.

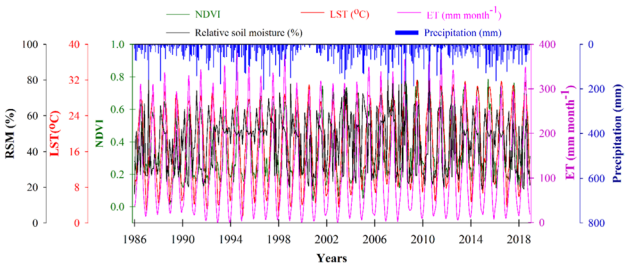

Fig. 5 Temporal variation of NDVI, LST, ET, Relative Soil Moisture (RSM), and precipitation from 1986 to 2018

Figure 7a shows the correlation between different variables including NVDI, LST, precipitation, RSM, and ET. Generally, the correlation among these variables ranged from -0.64 to 0.87. Notably, precipitation was found to be negatively correlated with NDVI, LST, RSM, and ET for most of the study area except for some areas in the North and Southwest. ET was mostly found to be positively associated with RSM, the opposite of the relationship found between precipitation and RSM. This was specifically true in the center part of the valley, where irrigation is heavily used to support crop production (Khan et al. 2019b). Hence, ET was found to capture the irrigation signals to represent absolute dryness and wetness over the agricultural area in the study area.

Figure 7b shows the spatial distribution of *p*-values from the correlation analysis showing the level of significance of the correlation between different environmental factors including precipitation, ET, NDVI, RSM, and LST. The exhibited correlation between different variables appears to be mostly significant across the majority of the study area, except for the relationship between precipitation with other variables. For most variables, *p*-values were less than 0.01, indicating significant positive or negative relationships (shown in Fig. 2) between these variables.

A significant increasing trend was observed for mean annual NDVI (Z = 4.66 and b = 0.004 and LST (Z = 3.57, b = 0.105), while annual ET, P, and RSM showed no significant trend from the year 1986 to 2018 (Table 2). Regarding ET, April ET and August ET showed a significant increasing trend. Notably, the increasing trend in August ET coincided with the significant increasing trend of August RSM, likely showing a positive contribution of RSM on ET.

Correlation between TVPDI and TVEPI with other remote sensing-based indices

The 3-month SPI and SSI temporal patterns resembled closely with those of TVEDI and TVPDI, more closely than the 6-month SPI and SSI (Fig. 8). Notably, the 3-month SPI and SSI values indicated a long dry spell (SPI or

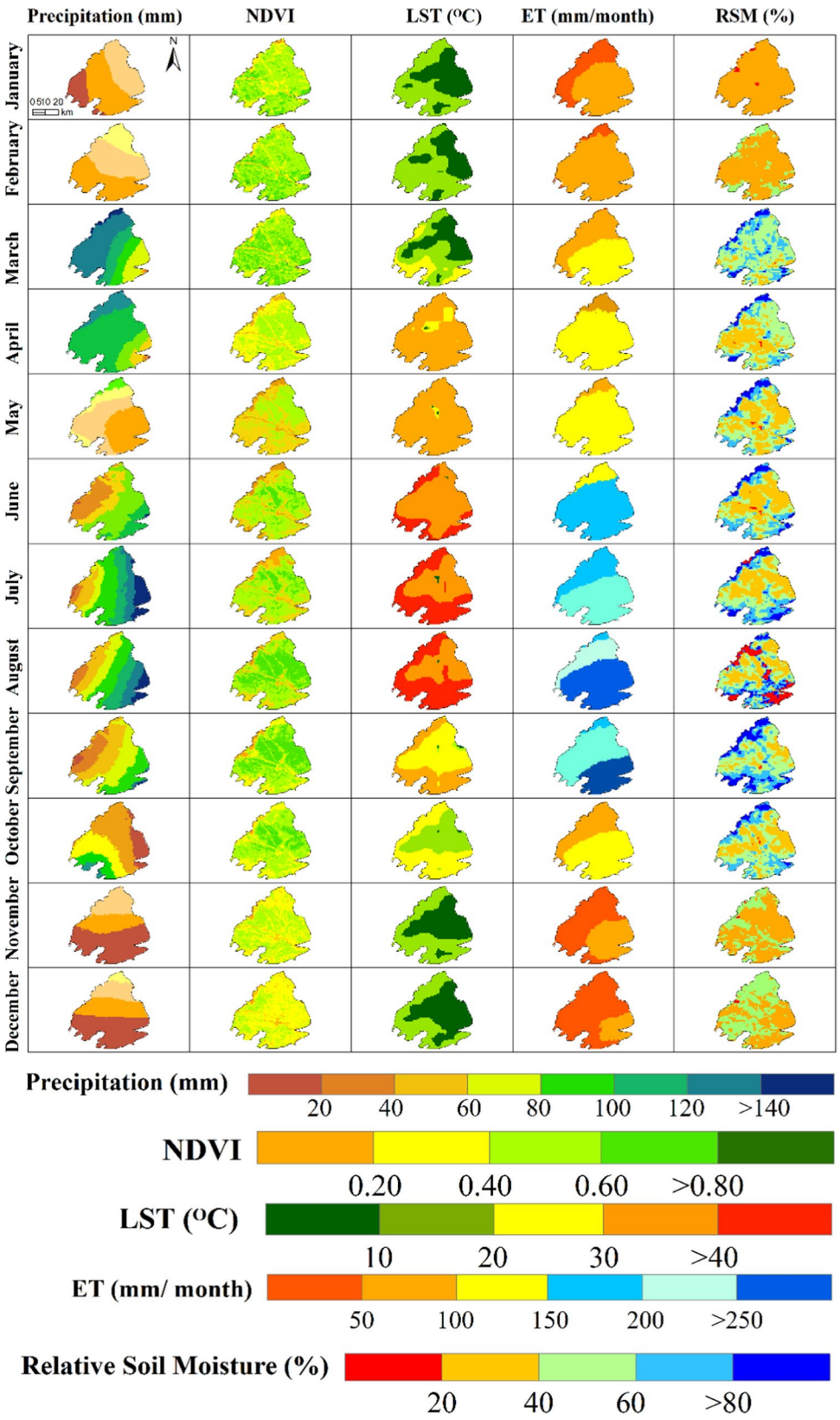

Fig. 6 Long-term (1986–2018) average precipitation, NDVI, LST, ET, and RSM

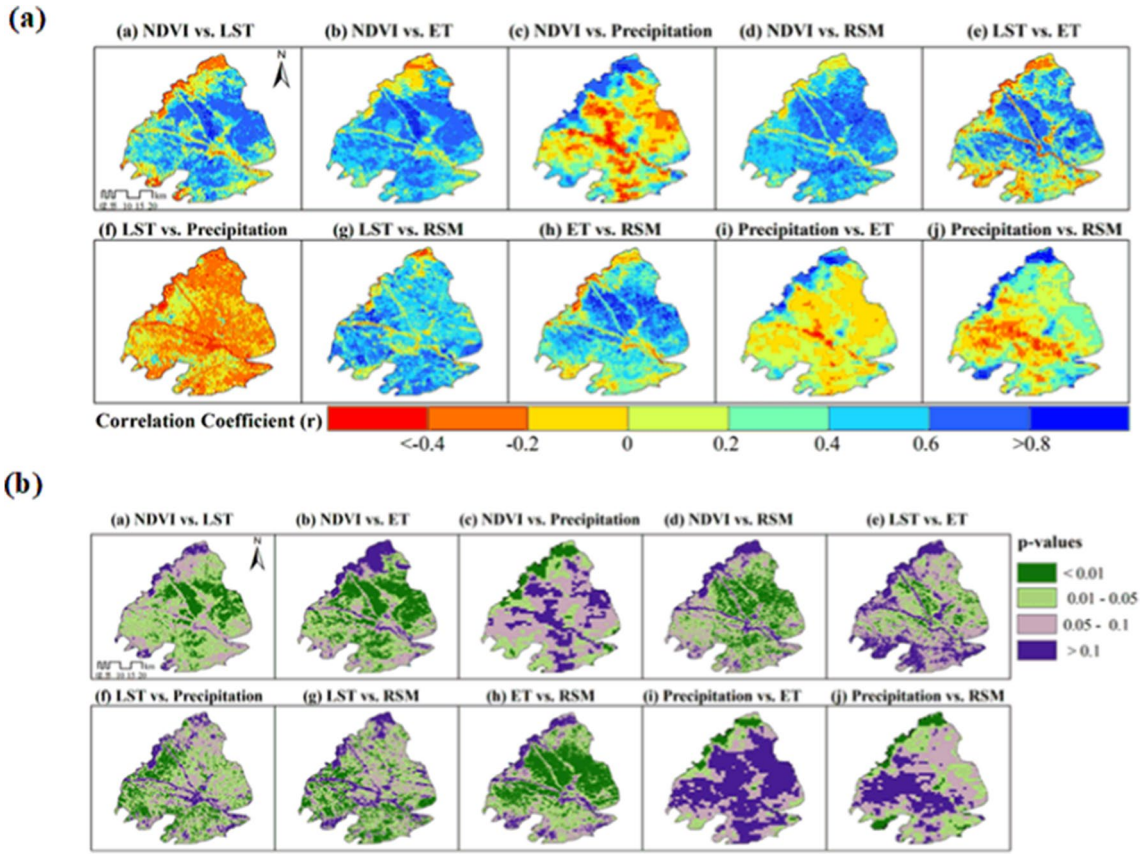

Fig. 7 The spatial distribution of the Pearson correlation (*r*) and *p*-values across the study area shows the level of significance of the correlation between NVDI, LST, precipitation, RSM, and ET

Table 2 Monthly and annual NDVI, LST, ET, precipitation, and RSM trends during 1986–2018 using the Modified Mann–Kendall test. Z, Sig., and b indicate Z-statistic, significance level (0.05), and Sen's Slope, respectively. Significance levels +, *, **, and *** indicate positive but not significant, marginally significant, and highly significant, respectively

Parameter	Test	Jan	Feb	Mar	Apr	May	Jun	Jul	Aug	Sep	Oct	Nov	Dec	Annual
NDVI	**Z**	0.85	-1.04	0.98	3.18	**3.30**	**3.41**	3.15	**4.01**	3.18	**4.11**	1.74	0.96	**4.66**
	Sig				**	***	***	**	***	**	***	+		***
	b	0.001	-0.001	0.001	0.003	0.007	0.007	0.005	0.006	0.005	0.005	0.001	0.001	0.004
LST	**Z**	1.22	0.53	1.18	3.02	3.18	2.40	**4.04**	2.60	3.18	1.57	0.89	1.60	**3.57**
	Sig				**	**	*	***	**	**	+		+	***
	b	0.102	0.125	0.072	0.094	0.091	0.053	0.101	0.114	0.119	0.164	0.154	0.142	0.105
ET	**Z**	-0.82	-1.47	-0.48	2.70	2.09	0.36	0.51	2.67	1.97	2.36	0.85	0.73	1.02
	Sig				**	*			**	*	*			
	b	-0.136	-0.095	-0.026	0.074	0.432	0.196	0.362	0.393	0.456	0.029	0.145	0.142	0.144
P	**Z**	-0.53	0.12	-2.28	-1.10	-0.23	1.02	1.94	1.50	1.32	-0.54	-0.90	-1.39	0.36
	Sig			*				+						
	b	-0.08	0.17	-0.80	-0.73	-0.11	0.30	0.051	0.104	0.58	-0.18	-0.09	-0.14	0.05
RSM	**Z**	-0.05	-0.23	-0.37	1.69	1.78	1.23	1.87	**3.82**	1.41	1.64	1.26	-0.78	0.98
	Sig				+	+		+	***		+			
	b	-0.021	-0.016	-0.321	0.254	0.17	0.028	0.616	0.133	0.295	0.118	0.300	-0.404	0.062

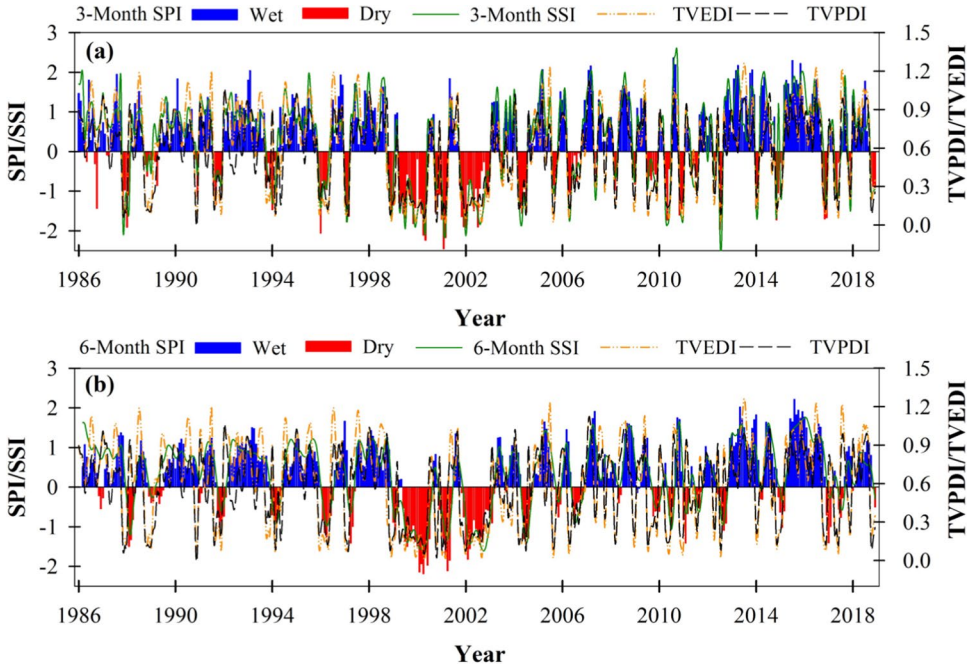

Fig. 8 Temporal variation of the TVEDI, TVPDI, SPI, and SSI at a) 3-month and b) six-month timescales from 1986 to 2018

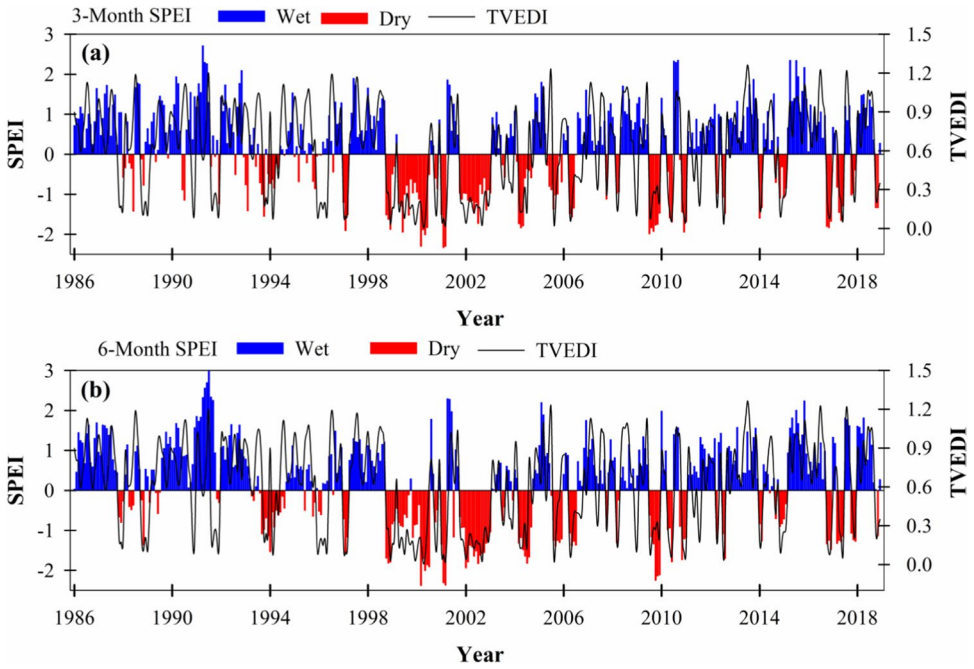

Fig. 9 Temporal variation of TVEDI and SPEI at a) 3-month and b) six-month timescales from 1986 to 2018

SSI = < -1) between 1999 and 2003, which was captured by TVEDI and TVPDI (TVEDI and TVPDI < 0.6). In addition, the 2015–2016 wet spell indicated by SPI and SSI (SPI or SSI > 1) was also captured well by TVEDI and TVPDI (TVEDI and TVPDI > 0.6).

The comparative analysis between SPEI and the TVEDI showed a strikingly similar association (Fig. 9). Both SPEI and TVEDI accurately predicted the occurrence of prolonged drought episodes during 1999–2001, and 2003–2004, spanning from 1986 to 2018. Moreover, the wet and average year's patterns exhibited a remarkable similarity between SPEI and TVEDI.

At both the 3-month and 6-month time scales, a positive association was observed between TVEDI and TVPDI with SPI, SSI, and SPEI. Notably, the correlation was stronger at the 3-month scale, as indicated in Table 3.

Table 3 Pearson correlation between SPI, SSI, SPEI, TVEDI, and TVPDI

Variables	3-Month SPI	3-Month SSI	3-Month SPEI	TVEDI
3-Month SSI	0.44			
3-Month SPEI	0.75	0.87		
TVEDI	0.78	0.82	0.84	
TVPDI	0.73	0.76	0.79	0.91
	6-Month SPI	6-Month SSI	6-Month SPEI	TVEDI
6-Month SSI	0.50			
6-Month SPEI	0.61	0.68		
TVEDI	0.44	0.52	0.71	
TVPDI	0.41	0.46	0.66	0.91

TVEDI displayed a slightly stronger correlation with SPI, SSI, and SPEI compared to TVPDI. For instance, the correlation coefficient between TVEDI and the 3-month SPI, SSI, and SPEI was 0.78, 0.82, and 0.84, respectively. These values were 6–7% higher than the correlation observed between TVPDI and the 3-month SPI and SSI. As anticipated, TVEDI and TVPDI exhibited a notably high correlation, with a coefficient of 0.91.

Spatial distributions of TVEDI and TVPDI during dry and wet years

The spatial distributions of TVEDI and TVPDI in dry (2000) and wet (2015) years are shown in Figs. 10a. In the dry year, TVEDI and TVPDI values showed a similar spatial pattern in the center part of the study area, but their spatial patterns were opposite or different in the North and South during the monsoon season (June–September). The most significant difference between the two was found in the Northern part of the valley during July 2000, when TVEDI values were ≤ 0.3, while TVPDI values were between ≤ 0.3–0.9. Similarly, in September 2000, in the southern part of the valley, TVPDI values were between ≤ 0.3 to 0.6, while TVEDI values were between 0.6 and 0.9.

In the wet year (2015), the spatial patterns of TVEDI and TVPDI were also similar (Fig. 10b). However, during the rabi growing season (October to April), they showed an opposite pattern, particularly in the central part of the country. For example, January TVEDI values in the center portion ranged between 0.3 and 0.6, while the TVPDI values were within 0.6–1.2.

Correlation between remote sensing variables, TVEDI, and TVPDI with crop yield

Seasonal yields from wheat and maize correlated well with the TVEDI and TVPDI from 1986–2018, with over two-thirds of the study area showing a positive correlation ($r > 0.3$; Fig. 11). This correlation was slightly higher with TVEDI, especially in the western and northern parts of the Peshawar Valley. TVEDI showed a higher correlation with the wheat yield than the maize yield, likely because the influence of precipitation was little during the dry season (November to March) when winter wheat is grown. In contrast, the southern part of the valley showed a higher correlation between maize yield and TVPDI than the TVEDI, which could be due to higher precipitation in the monsoon season when maize is grown (Khan et al. 2020). Overall, a higher correlation with crop yield indicates that TVEDI may have a slight advantage over TVPDI in terms of monitoring drought in irrigated areas.

Figure 12 shows the spatial distribution of *p*-values and the significance levels of the correlation between TVEDI and TVPDI with maize and wheat yields. A larger portion of the study area showed a significant relationship (p-value < 0.05) between TVEDI and crop yields, compared to the correlation between TVPDI and crop yields. This suggests a broader and more significant relationship of TVEDI with crop yields, highlighting the enhanced ability of TVEDI in agricultural drought assessments.

Discussion

TVEDI is a new composite index derived by modifying the existing TVDPI index, where precipitation is substituted with ET. This is analogous to how SPI was modified into SPEI but in the case of TVEDI, actual ET is used. The primary motivation for using ET is that it provides a more accurate measure of water stress on crops and captures the stomatal responses of crops. During drought, crops often respond by closing their stomata, a natural adaptation to reduce transpiration rates and conserve water resources (Guha et al. 2018). This physiological response becomes particularly evident in agricultural regions, where prolonged droughts can lead to either crop mortality or severe stunting of foliage growth. As a result, the plant's ability to transpire water is significantly hindered (Morton et al. 2013; Salimi et al. 2021). This detrimental effect on crop health inevitably translates into reduced crop yields. As such, TVEDI showed a higher correlation with crop yield than the TVDPI. Hence, TVEDI's superior performance can be attributed to its incorporation of ET, while TVPDI primarily relies on precipitation data, overlooking critical factors like soil moisture and ET.

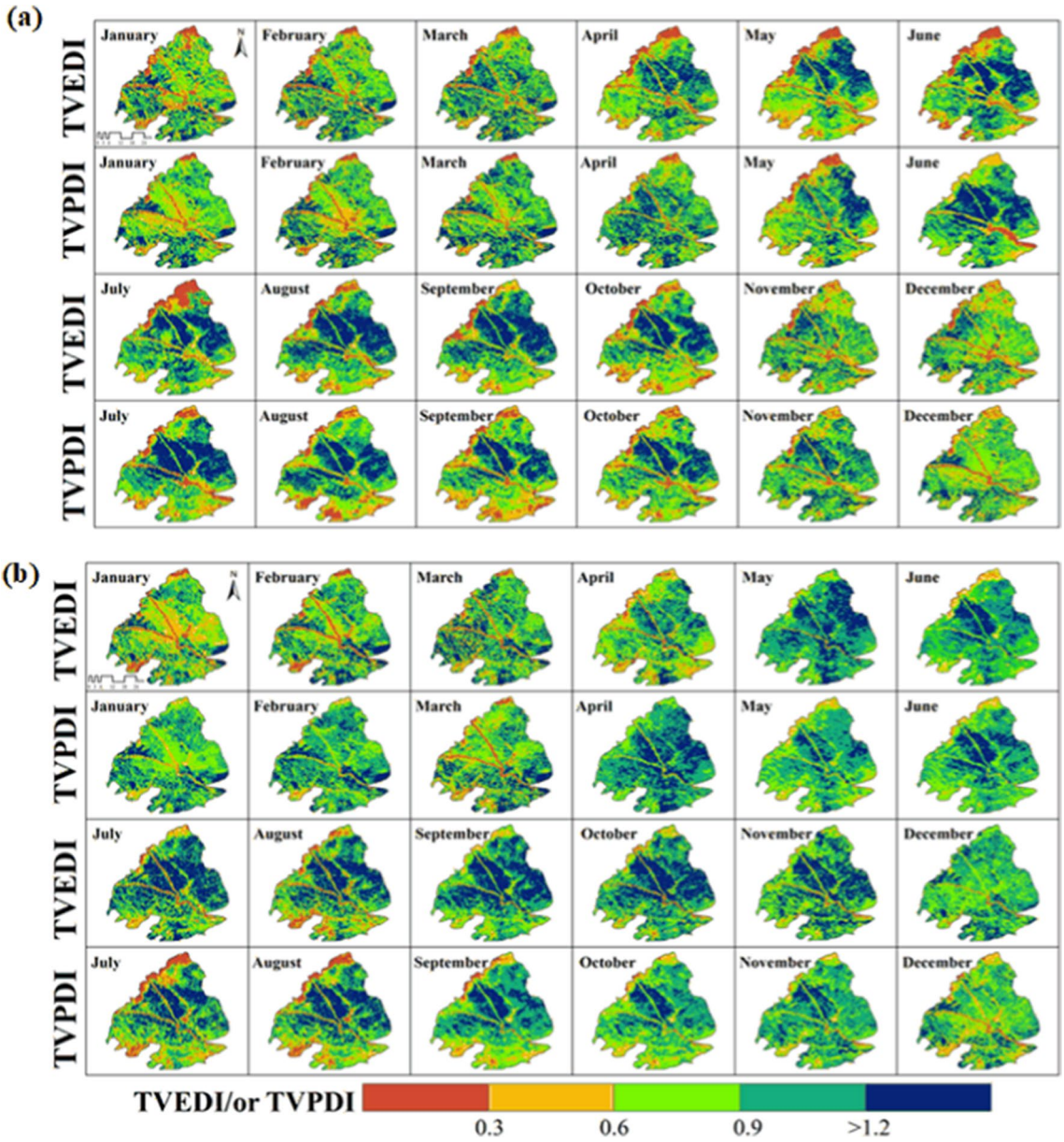

Fig. 10 Spatial patterns of TVEDI and TVPDI showing dry and wet areas during the dry year (2000) and wet year (2015)

It is essential to recognize that traditional precipitation-based drought indices may not accurately capture the real water stress conditions experienced by crops in irrigated areas (Javed et al. 2021a). This limitation arises from their inability to account for the actual water consumed by crops, as they are solely based on precipitation data. To address this limitation, remotely sensed ET can directly assess crop water consumption, offering a more precise indicator of water stress. Furthermore, including additional variables, such as LST and NDVI, in TVEDI significantly enhances its ability to detect drought conditions. LST can effectively capture surface dryness (Baig et al. 2020), while NDVI provides valuable insights into vegetation health and conditions (Tan et al. 2012; Yue et al. 2007). These supplementary factors contribute to the comprehensiveness of TVEDI as an index for monitoring agricultural drought, particularly in regions heavily reliant on irrigation practices.

TVEDI also showed a stronger positive correlation with widely recognized meteorological drought indices (SPI, SPEI, and SSI) than TVPDI. This implies that TVEDI can capture soil moisture fluctuations and meteorological drought conditions, particularly when these conditions impact crop health. Commonly used drought indices also have a limited ability to capture agricultural drought and crop responses. For example, SPI is solely precipitation-based, potentially inadequately characterizing agricultural

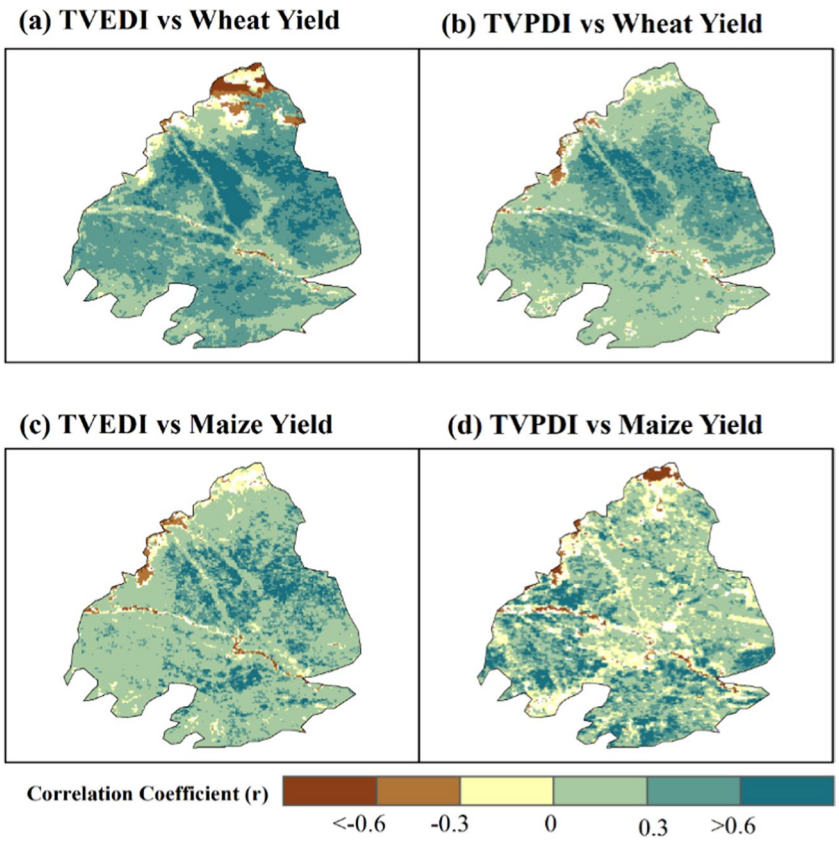

Fig. 11 Pearson correlation (*r*) values between the crop yield vs. TVEDI and TVPDI from 1986–2018

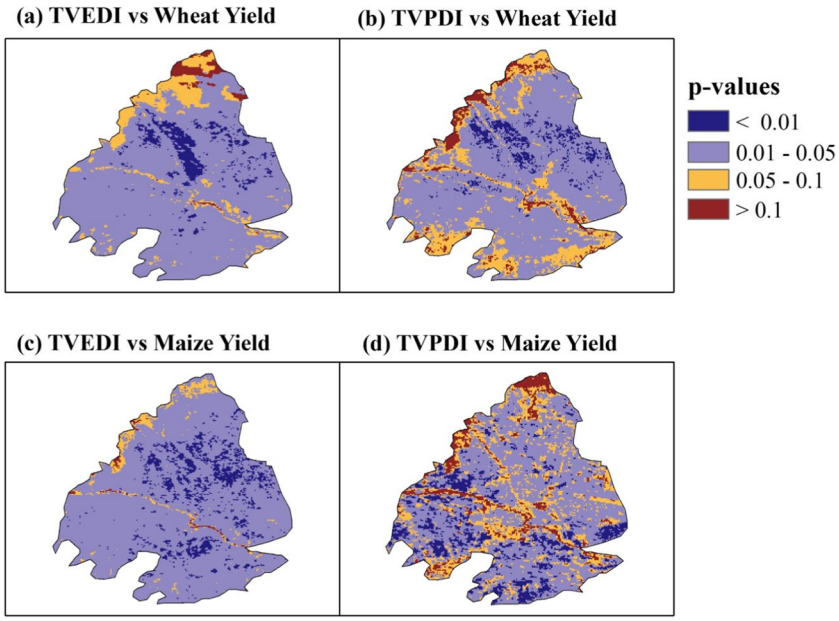

Fig. 12 The spatial distribution of the *p*-values across the study area showing the level of significance of the correlation between TVEDI and TVPDI with crop yields

drought in regions where temperature and soil moisture are significant factors. Some of these commonly used indices have limited applicability. For example, SSI relies on soil moisture data, which may not be consistently available or account for variations in soil properties, limiting its applicability and spatial coverage for drought assessment. TVEDI offers a more comprehensive approach to drought assessment, making it a promising tool for monitoring agricultural drought, where diverse factors come into play (Ying et al. 2023b; Chen et al. 2020).

We find that TVEDI can be an effective tool for monitoring agricultural drought, particularly in areas where

irrigation plays a significant role. Its incorporation of ET, utilization of remotely sensed data, and consideration of LST and NDVI collectively make it a valuable tool for assessing crop water stress and drought conditions. Nonetheless, it is essential to further refine and enhance drought monitoring approaches, considering the diverse agricultural and environmental contexts. In addition, it is constrained by the availability of remotely sensed data and their spatial and temporal resolution, potentially limiting its ability to capture localized or short-term drought events and failing to account for specific regional or crop characteristics. Fortunately, with recent advancements in ET monitoring using remotely sensed data and the availability of multiple-source ET products (Bhattarai and Wagle 2021; Hu et al. 2023), our ability to monitor agricultural drought and assess its impacts using an ET-based drought index is expected to advance in future. Overall, the results from this study underscore the importance of using multiple remote sensing variables in agricultural drought monitoring, as a single variable may not precisely predict agricultural drought due to the complex nature of crop responses to drought and water availability.

Conclusion

To address the limited ability of common remotely sensed products like NDVI, LST, ET, RSM, and precipitation in accurately identifying agricultural drought, this study integrated these products and modified the TVPDI to develop a new index called TVEDI. To address the challenges posed by limited data availability in data-scarce, yet drought-prone regions like the Peshawar valley in Pakistan, remotely sensed data, particularly ET derived from Landsat from 1986 to 2018, was integrated into TVEDI. This index was found to be highly correlated with common drought indices (e.g., SPI, SPEI, and SSI) and crop growth indicators (crop yield). In most cases, these correlations were found to be stronger and more widely distributed than those from TVPDI. Moreover, TVEDI performed better at predicting dryness across agricultural regions and correlated much more strongly with crop yield than TVPDI. Overall, TVEDI, a new satellite-based integrated dryness index, characterized agricultural drought well across our study region in Pakistan. Future research should investigate the performance of TVEDI in characterizing agricultural drought across a wide range of geographic regions.

Acknowledgements The authors appreciate the anonymous reviewers and the editors for their valuable comments for significantly improving this manuscript.

Author contribution Each author's assistance to the article is as follows: Jiahua Zhang, and Nishan Bhattarai conceptualization and supervision; Tehseen Javed, conceptualization, formal analysis, investigation, methodology, writing original draft, writing review and editing, software, and validation; Tehseen Javed and Jiahua Zhang, writing original draft, project administration, resources, and funding acquisition; Nishan Bhattarai and Bharat Sharma Acharya, investigation, data curation, and resources. Every author has made significant contributions.

Funding This work was jointly supported by the Central Guiding Local Science and Technology Development Fund of Shandong-Yellow River Basin Collaborative Science and Technology Innovation Special Project (No. YDZX2023019), Natural Science Foundation of China (No. 42071425), Shandong Natural Science Foundation of China (No. ZR2023QD073, No. ZR2020QE281).

Data availability The data will be available on request.

Declarations

Ethics approval and consent to participate This research does not involve human or animal trials.

Consent for publication The author grants the publisher the sole and exclusive license of the full copyright in the contribution, which licenses the publisher hereby accepts.

Competing interests The authors declare no competing interests.

References

Abramowitz M, Stegun IA (Eds.) (1965) Handbook of mathematical functions with formulas, graphs, and mathematical tables. Dover Publications Inc., New York, p 1046

Allen RG et al (2007) Satellite-based energy balance for mapping evapotranspiration with internalized calibration (METRIC)—Applications. J Irrig Drain Eng 133(4):395–406

Anderson MC, Allen RG, Morse A, Kustas WP (2012) Use of Landsat thermal imagery in monitoring evapotranspiration and managing water resources. Remote Sens Environ 122:50–65. https://doi.org/10.1016/j.rse.2011.08.025

Anderson MC, Zolin CA, Sentelhas PC, Hain CR, Semmens K, Yilmaz MT, Gao F, Otkin JA, Tetrault R (2016) The Evaporative Stress Index as an indicator of agricultural drought in Brazil: An assessment based on crop yield impacts. Remote Sens Environ 174:82–99

Baig MHA et al (2020) Assessing meteorological and agricultural drought in Chitral Kabul river basin using multiple drought indices. Remote Sens 12(9):1417

Bhattarai N, Wagle P (2021) Recent advances in remote sensing of evapotranspiration. Remote Sens 13(21):4260

Bhattarai N, Shaw SB, Quackenbush LJ, Im J, Niraula R (2016) Evaluating five remote sensing-based single-source surface energy balance models for estimating daily evapotranspiration rates in a humid subtropical climate. Int J Appl Earth Obs Geoinf 49:75–86

Bhattarai N, Wagle P, Gowda P, Kakani V (2017) Utility of remote sensing-based surface energy balance models to track water stress in rain-fed switchgrass under dry and wet conditions. ISPRS J Photogramm Remote Sens 133:128–141

Bhattarai N, Mallick K, Brunsell NA, Sun G, Jain M (2018) Regional evapotranspiration from an image-based implementation of the Surface Temperature Initiated Closure (STIC1. 2) model and its validation across an aridity gradient in the conterminous US. Hydrol Earth Syst Sci 22(4):2311–2341

Bhattarai N, Mallick K, Stuart J, Vishwakarma BD, Niraula R, Sen S, Jain M (2019) An automated multi-model evapotranspiration mapping framework using remotely sensed and reanalysis data. Remote Sens Environ 229:69–92

Brutsaert W (1999) Aspects of bulk atmospheric boundary layer similarity under free-convective conditions. Rev Geophys 37(4):439–451. https://doi.org/10.1029/1999RG900013

Businger JA et al (1971) Flux-profile relationships in the atmospheric surface layer. Journal of the Atmospheric Sciences 28:181–189. https://doi.org/10.1175/1520-0469(1971)028<0181:FPRITA>2.0.CO;2

Chen X et al (2020) Impacts of multi-timescale SPEI and SMDI variations on winter wheat yields. Agric Syst 185:102955

Chen L, Li M, Huang F, Xu S (2013) Relationships of LST to NDBI and NDVI in Wuhan City based on Landsat ETM+ image, 6th International Congress on Image and Signal Processing (CISP), Hangzhou, China, 2013, pp. 840-845. https://doi.org/10.1109/CISP.2013.6745282

Danielsson P-E (1980) Euclidean distance mapping. Comput Graphics Image Process 14(3):227–248

dos Santos BC, Sanches RG, de Melo Bolleli T, de Souza PH, Bourscheidt V (2022) Satellite-Based Precipitation Estimates Validation Using Surface Stations in the Central Region of the State of São Paulo, From 1981 to 2019, 10 January 2022, PREPRINT (Version 1) available at Research Square. https://doi.org/10.21203/rs.3.rs-1153248/v1

Edwards C, McKee T, Doesken N, Kleist J (1997) Historical analysis of drought in the United States. Seventh Conference on Climate Variations, 77th AMS Meeting, Long Beach, California, 2-7 February 1997, pp 129–139

Fadholi A, Adzani R (2018) Analisis frekuensi curah hujan ekstrem kepulauan bangka belitung berbasis data climate hazards group infra-red precipitation with stations (CHIRPS). Gea: Jurnal Pendidikan Geografi 18(1). https://doi.org/10.17509/gea.v18i1.9504

FAO, (Food and Agriculture Organization) (2009) CROPWAT Software, Food and Agriculture Organization, Land and Water Division; Available at: http://www.fao.org/nr/water/infores_databases_cropwat.html

Fatemi M, Narangifard M (2019) Monitoring LULC changes and its impact on the LSand NDVI in District 1 of Shiraz City. Arab J Geosci 12(4):1–12

Govil H, Guha S, Diwan P, Gill N, Dey A (2020) Analyzing linear relationships of LST with NDVI and MNDISI using various resolution levels of landsat 8 OLI and TIRS data. In: Sharma N, Chakrabarti A, Balas V (eds) Data management, analytics and innovation. Adv Intell Syst Comput 1042:171–184. https://doi.org/10.1007/978-981-32-9949-8_13

Guha S, Govil H, Dey A, Gill N (2018) Analytical study of land surface temperature with NDVI and NDBI using Landsat 8 OLI and TIRS data in Florence and Naples city, Italy. Eur J Remote Sens 51(1):667–678

Hao Z, AghaKouchak A (2013) Multivariate standardized drought index: a parametric multi-index model. Adv Water Resour 57:12–18

He R, Jin Y, Kandelous MM, Zaccaria D, Sanden BL, Snyder RL, Jiang J, Hopmans JW (2017) Evapotranspiration Estimate over an Almond Orchard Using Landsat Satellite Observations. Remote Sens 9(5):436. https://doi.org/10.3390/rs9050436

Henchiri M et al (2020) Spatio-temporal patterns of drought and impact on vegetation in North and West Africa based on multi-satellite data. Remote Sens 12(23):3869

Hu T, Mallick K, Hitzelberger P, Didry Y, Boulet G, Szantoi Z et al (2023) Evaluating european ECOSTRESS hub evapotranspiration products across a range of soil-atmospheric aridity and biomes over Europe. Water Resources Research 59:e2022WR034132. https://doi.org/10.1029/2022WR034132

Hussain M et al (2021) GIS-Based Multi-Criteria Approach for Flood Vulnerability Assessment and Mapping in District Shangla: Khyber Pakhtunkhwa, Pakistan. Sustainability 13(6):3126

IPCC (2021) Climate Change 2021: The physical science basis. Contribution of working group I to the sixth assessment report of the intergovernmental panel on climate change. Cambridge, UK: Cambridge University Press

Jaafar HH, Ahmad FA (2020) Time series trends of Landsat-based ET using automated calibration in METRIC and SEBAL: The Bekaa Valley, Lebanon. Remote Sens Environ 238:111034

Javed T, Yao N, Chen X, Suon S, Li Y (2020) Drought evolution indicated by meteorological and remote-sensing drought indices under different land cover types in China. Environ Sci Pollut Res 27(4):4258–4274

Javed T et al (2021a) Performance and relationship of four different agricultural drought indices for drought monitoring in China's mainland using remote sensing data. Sci Total Environ 759:143530

Javed T et al (2021b) Drought characterization across agricultural regions of China using standardized precipitation and vegetation water supply indices. J Clean Prod 313:127866. https://doi.org/10.1016/j.jclepro.2021.127866

Kendall M (1976) Rank Auto Correlation Methods, 4th edn. Griffin, Oxford

Khan A et al (2019a) Estimating biomass and yield using metric evapotranspiration and simple growth algorithms. Agron J 111(2):536–544

Khan I et al (2019b) Impact assessment of land use change on surface temperature and agricultural productivity in Peshawar-Pakistan. Environ Sci Pollut Res 26(32):33076–33085

Khan I et al (2020) Farm households' risk perception, attitude and adaptation strategies in dealing with climate change: promise and perils from rural Pakistan. Land Use Policy 91:104395

Kwon M, Kwon HH, Han D (2019) Spatio-temporal drought patterns of multiple drought indices based on precipitation and soil moisture: A case study in South Korea. Int J Climatol 39(12):4669–4687

Liu Q, Zhang S, Zhang H, Bai Y, Zhang J (2020) Monitoring drought using composite drought indices based on remote sensing. Sci Total Environ 711:134585

Liu Q et al (2021) Evaluating the performance of eight drought indices for capturing soil moisture dynamics in various vegetation regions over China. Sci Total Environ 789:147803

Madugundu R, Al-Gaadi KA, Tola E, Hassaballa AA, Patil VC (2017) Performance of the METRIC model in estimating evapotranspiration fluxes over an irrigated field in Saudi Arabia using Landsat-8 images. Hydrol Earth Syst Sci 21(12):6135–6151

Mann HB (1945) Non-parametric test against trend. Econometrica 13:245-259. https://doi.org/10.2307/1907187

Mishra AK, Singh VP (2010) A review of drought concepts. J Hydrol 391(1–2):202–216

Morton CG et al (2013) Assessing calibration uncertainty and automation for estimating evapotranspiration from agricultural areas using METRIC. JAWRA J Am Water Resour Assoc 49(3):549–562

Musie M, Sen S, Srivastava P (2019) Comparison and evaluation of gridded precipitation datasets for streamflow simulation in data scarce watersheds of Ethiopia. J Hydrol 579:124168

Numata I, Khand K, Kjaersgaard J, Cochrane MA, Silva SS (2017) Evaluation of Landsat-based METRIC modeling to provide high-spatial resolution evapotranspiration estimates for Amazonian forests. Remote Sens 9(1):46

Pachauri RK et al (2014) Climate change 2014 synthesis report. contribution of working groups I, II, and III to the fifth assessment report of the Intergovernmental Panel on Climate Change. IPCC. http://www.mendeley.com/research/climate-change-2014-synth

esis-report-contribution-working-groups-i-ii-iii-fifth-assessment-report-in-20
Salimi H, Asadi E, Darbandi S (2021) Meteorological and hydrological drought monitoring using several drought indices. Appl Water Sci 11(2):1–10
Senay GB, Friedrichs M, Singh RK, Velpuri NM (2016) Evaluating Landsat 8 evapotranspiration for water use mapping in the Colorado River Basin. Remote Sens Environ 185:171–185
Sims AP, Niyogi DdS, Raman S (2002) Adopting drought indices for estimating soil moisture: A North Carolina case study. Geophys Res Lett 29(8):24-1–24-4
Soľáková T, De Michele C, Vezzoli R (2014) Comparison between parametric and nonparametric approaches for the calculation of two drought indices: SPI and SSI. J Hydrol Eng 19(9):04014010
Tan KC, San Lim H, MatJafri MZ, Abdullah K (2012) A comparison of radiometric correction techniques in the evaluation of the relationship between LST and NDVI in Landsat imagery. Environ Monit Assess 184(6):3813–3829
Tasumi M (2019) Estimating evapotranspiration using METRIC model and Landsat data for better understandings of regional hydrology in the western Urmia Lake Basin. Agric Water Manag 226:105805
Thom HC (1958) A note on the gamma distribution. Mon Weather Rev 86(4):117–122
Vicente-Serrano SM, Beguería S, López-Moreno JI (2010) A Multiscalar Drought Index Sensitive to Global Warming: The Standardized Precipitation Evapotranspiration Index. J Climate 23:1696–1718. https://doi.org/10.1175/2009JCLI2909.1
Vicente-Serrano SM et al (2012) Performance of drought indices for ecological, agricultural, and hydrological applications. Earth Interact 16(10):1–27
Wang L, Zhang Y, Feng J (2005) On the Euclidean distance of images. IEEE Trans Pattern Anal Mach Intell 27(8):1334–1339
Wei W et al (2020) Temperature vegetation precipitation dryness index (TVPDI)-based dryness-wetness monitoring in China. Remote Sens Environ 248:111957
Yang Y, Anderson MC, Gao F, Wardlow B, Hain CR, Otkin JA, Alfieri J, Yang Y, Sun L, Dulaney W (2018) Field-scale mapping of evaporative stress indicators of crop yield: An application over Mead, NE, USA. Remote Sens Environ 210:387–402
Ying L, Fuzhen S, Hui Y, Xu W (2023) Characteristics of drought propagation and effects of water resources on vegetation in the karst area of Southwest China. Sci Total Environ (891): ISSN 0048–9697. https://doi.org/10.1016/j.scitotenv.2023.164663
Ying L, Fuzhen S, Hui Y, Xu W, Yahui F (2023) Global analysis of the correlation and propagation among meteorological, agricultural, surface water, and groundwater droughts. J Environ Manag (333): ISSN 0301–4797. https://doi.org/10.1016/j.jenvman.2023.117460
Yue S, Wang CY (2002) Applicability of prewhitening to eliminate the influence of serial correlation on the Mann-Kendall test. Water Resour Res 38(6):4-1–4-7
Yue W, Xu J, Tan W, Xu L (2007) The relationship between land surface temperature and NDVI with remote sensing: application to Shanghai Landsat 7 ETM+ data. Int J Remote Sens 28(15):3205–3226
Zheng G, Monika Moskal L (2009) Retrieving Leaf Area Index (LAI) Using Remote Sensing: Theories, Methods and Sensors. Sensors 9(4):2719–2745. https://doi.org/10.3390/s90402719

Publisher's Note Springer Nature remains neutral with regard to jurisdictional claims in published maps and institutional affiliations.

Springer Nature or its licensor (e.g. a society or other partner) holds exclusive rights to this article under a publishing agreement with the author(s) or other rightsholder(s); author self-archiving of the accepted manuscript version of this article is solely governed by the terms of such publishing agreement and applicable law.